HOKKAIDO UNIVERSITY

Title	Directional Characteristics and Forms of the Detector Surface in Optical Heterodyne Detection Processes
Author(s)	Sakuraba, Ichiro; Tsubo, Toshihiro
Citation	Memoirs of the Faculty of Engineering, Hokkaido University, 12(3), 295-318
Issue Date	1969-01
Doc URL	http://hdl.handle.net/2115/37859
Type	bulletin (article)
File Information	12(3)_295-318.pdf

Instructions for use

Hokkaido University Collection of Scholarly and Academic Papers : HUSCAP

Directional Characteristics and Forms of the Detector Surface in Optical Heterodyne Detection Processes

Ichiro SAKURABA
Toshihiro TSUBO
Department of Electronic Engineering
Faculty of Engineering
Hokkaido University, Sapporo, Japan

(Received August 28, 1968)

Contents

Abstract 295
1. Introduction 296
2. General Solution 297
3. Unfocused Light 298
3.1. The Rectangular Surface 300
3.2. The Circular Surface 303
4. Focused Beams 305
4.1. Beams Focused by a Single Aperture 305
4.2. Beams Focused by Two Apertures 309
5. A Comparison of Theoretical and Experimental Values 314
6. Conclusions 317
Acknowledgment 317
References 317

Abstract

In optical heterodyne detection processes, Corcoran's analysis on the directional characteristics of one-dimensional detectors was modified to two-dimensional detectors.

In the case of unfocused light beams the directivity factor of a rectangular detector of sides a and b, $D(\theta_1, \theta_2, \varphi_1, \varphi_2)$, is given by $4\sin(pa/2)\cdot\sin(qb/2)/pqab$ and the directivity factor of a circular detector with a radius of ρ_0 is $D(\omega, \rho_0) = 2J_1(\omega, \rho_0)/\omega\rho_0$. The directivity factor of focusing light beams with a single rectangular aperture of sides ξ_a and η_a is in a similar form to the unfocused Fraunhofer problem and the directional pattern is narrowed as the rectangular aperture is increased. In a case where two rectangular apertures are used and translated so that the images remain fixed as the angle of incidence changes, the directional pattern is less sensitive to the angle.

Good experimental confirmation was obtained with optical homodyne receivers.

1. Introduction

The fundamental properties of optical heterodyning as a coherent optical detection method were fairly well presented by Hutter[1], Jacobs[2], Siegman, Harris, McMurtry[3], Sakuraba and Rowe[4),5),6]. The signal and noise properties of optical heterodyne receivers have been discussed thoroughly by Oliver[7], Haus, Townes, Oliver[8], Jacobs, Rabinowitz, LaTourrette and Gould[9),10]. The strict alignment tolerances necessary to keep signal and local oscillator wavefronts in phase, over the photosensitive surface have also been pointed out by Siegman, Harris, McMurtry[3], Corcoran[11], Sakuraba and Chida[12] and directions for apparently relaxing these alignment tolerances have been offered by Read, Fried and Turner[13),14] and the antenna properties of optical heterodyne receivers were pointed out by Siegman[15]. The optical superheterodyne receiver which uses a precision angle tracking servo to maintain receiver spatial alignment with a remote transmitter was recently shown by Lucy, Lang, Peters and Duval[16].

The optical heterodyning exhibts selectivity properties which do not normally appear in heterodyne detection at lower frequencies. These directional properties arise because the surface or detector volume is generally large compared to the optical wave length. As a result, the phase difference between two light beams and thus the phase of the difference frequency signal, can vary widely over the detector surface. In previous work on optical heterodyne detection, directional problems have been mentioned but no quantitative results have been given in detail.

Corcoran[11] gave the directional characteristics of the one-dimensional strip detector in the case of two unfocused light beams, focusing light beams with a single aperture and focusing beams with multiple apertures. It was shown in his analysis that when the effective aperture is increased by focusing two beams with a single lens, then the directivity increases, but if two apertures are used in order to maintain the images in the same position, the directivity is reduced. In order to determine the directional characteristics in a heterodyne detection process, the distribution of the radiation at the detector surface and the shape of the detector surface must be considered.

This paper deals with the directional characteristics of two-dimensional detectors in optical heterodyne detection processes. The derivation will be based on Corcoran's analysis for one-dimensional detectors and information will be added by extending his analysis to two-dimensional detectors. A comparison of theoretical and experimental values will be made with rectangular and circular detectors in optical homodyne receivers.

2. General Solution

Analyses of the photodetection mechanism for incoherent and coherent radiation[17),18)] have shown that the current output of the detector is proportional to the square of the total electric field at each point on the detection surface. This was summed up over the entire area, and temporally averaged over a short period of time (10^{-10} sec for a photoelectric material)[19)]. Then the output current of the detector process can be expressed as

$$\begin{aligned} i(t) &= \frac{1}{T}\int_{t-T}^{T}\int_{A}\left[V^{(r)}(P,t')\right]^2 dA dt' \\ &= \frac{1}{4T}\int_{t-T'}^{T}\int_{A}[V^2+2VV^*+V^{*2}]dA\cdot dt' \\ &= \frac{1}{2}\int_{A}\langle VV^*\rangle dA+\frac{1}{4}\int_{A}\langle V^2+V^{*2}\rangle dA\,, \end{aligned} \tag{1}$$

where $V^{(r)}(P,t)$ is the real disturbance at point P and time t proportional to a component of the electric field[20)] and $V(P,t)$ is the complex function associated with $V^{(r)}(P,t)$. An unessential constant factor has been dropped and the brackets indicate a time average over an interval T around t. When the field at the detector surface is a superposition of monochromatic waves:

$$V(P,t)=\sum_{n}E_n(P)e^{-j\omega_n t} \tag{2}$$

the output current is

$$\begin{aligned} i(t) &= \frac{1}{2}\int_{A}\langle\sum_{n}E_n(P)\cdot E_n^*(P)\rangle dA+\frac{1}{2}\int_{A}\langle\sum_{\substack{mn\\ m\neq n}}E_n(P)\cdot E_m^*(P)e^{-j(\omega_n-\omega_m)t}\rangle dA \\ &\quad+\frac{1}{4}\int_{A}\langle(\sum_{n}E_n(P)e^{-j\omega_n t})^2+(\sum_{n}E_n^*(P)e^{j\omega_n t})^2\rangle dA\,. \end{aligned} \tag{3}$$

The first term shows the d-c current and the third term has optical frequency terms. It is noted that optical frequency terms are presumably completely suppressed by the averaging process. Even if they were not, we have no practical means of coupling or measuring an optical-frequency-modulated electron current. Then the output current becomes

$$\begin{aligned} i(t) &= \frac{1}{2}\int_{A}\langle\sum_{\substack{m,n\\ m\neq n}}E_n(P)\cdot E_n^*(P)e^{-j(\omega_n-\omega_m)t}\rangle dA \\ &= K\sum_{\substack{m,n\\ m\neq n}}e^{-j(\omega_n-\omega_m)t}\int_{A}E_n(P)\cdot E_n^*(P)dA\,, \end{aligned} \tag{4}$$

where an average was taken over a period so that

$$\omega_n - \omega_m < 1/T < \omega_n, \omega_m, \tag{5}$$

and the average value of the current was ignored. Since n and m assume all values, the expression for the current can be written as

$$i(t) = \mathrm{Re} \sum_{\substack{m,n \\ m>n}} e^{-j(\omega_n - \omega_m)t} \int_A E_n \cdot E_m^* dA . \tag{6}$$

Again, the unessential constant factor was ignored.

In particular when the field at P is due to the superposition of two waves,

$$i(t) = \mathrm{Re}\, e^{-j(\omega_1 - \omega_2)t} \int E_1 \cdot E_2^* dA . \tag{7}$$

With a knowledge of the spatial variation of the electric field across the detection surface, the output current for the problems of interest can be calculated from Eq. (7).

3. Unfocused Light

A schematic representation of the problem of detecting two unfocused light beams is shown in Figs. 1 and 2. Two light beams emanating from points P_{01} (X_{01}, Y_{01}, Z_{01}) and P_{02} (X_{02}, Y_{02}, Z_{02}) are superimposed at the detector surface. The detector is centered at $x=y=0$ in the plane $z=0$. The light from P_{01} and P_{02} is assumed

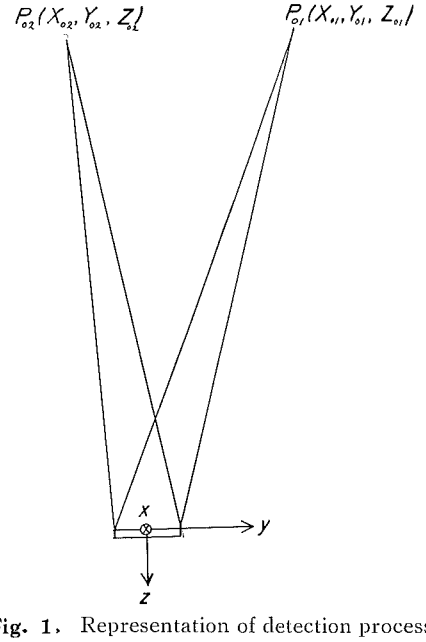

Fig. 1. Representation of detection process with unfocused light.

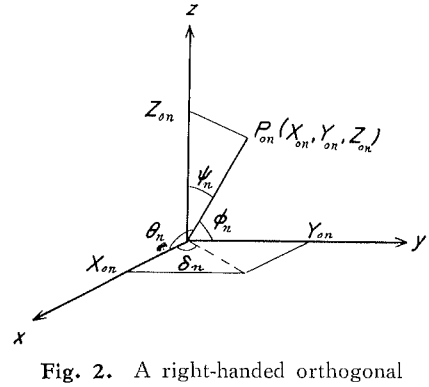

Fig. 2. A right-handed orthogonal system.

to propagate in the form of spherical waves, and the distances r_1 and r_2 from each source to any point on the detector is such that the $1/r$ variation is negligible. With these assumptions, the field at $\mathrm{P}(x, y, 0)$ on the detection surface is given by

$$V(P, t) = E_1 e^{-j\omega_1 t} + E_2 e^{-j\omega_2 t}, \tag{8}$$

where

$$E_1 = A_1 e^{jk_1 r_1}, \qquad E_2 = A_2 e^{jk_2 r_2}. \tag{9}$$

The distance from a point P_{0n} to a point P on the detector is

$$\begin{aligned} r_n &= \left[(x-X_{0n})^2+(y-Y_{0n})^2+Z_{0n}^2\right]^{1/2} \\ &= \left[r_n'^2-2xX_{0n}-2y\,Y_{0n}+x^2+y^2\right]^{1/2}, \end{aligned} \tag{10}$$

where

$$r_n'^2 = X_{0n}^2 + Y_{0n}^2 + Z_{0n}^2. \tag{11}$$

Since the linear dimension of the detector is small compared to r_n', r_n can be expanded by means of the binominal theorem. The result is

$$\begin{aligned} r_n &= \left[r_n'^2+(x^2+y^2-2xX_{0n}-2yY_{0n})\right]^{1/2} \\ &= r_n' + \frac{1}{2}(r_n')^{-1}(x^2+y^2-2xX_{0n}-2yY_{0n}) \\ &\quad -\frac{1}{8}(r_n')^{-3}(x^2+y^2-2xX_{0n}-2yY_{0n})+\cdots \\ &\cong r_n' - x\cos\theta_n - y\cos\varphi_n + \frac{x^2}{2r_n'}\sin^2\theta_n + \frac{y^2}{2r_n'}\sin^2\varphi_n + \cdots, \end{aligned} \tag{12}$$

where

$$\theta_n = \cos^{-1}(X_{0n}/r_n'), \qquad \varphi_n = \cos^{-1}(Y_{0n}/r_n'). \tag{13}$$

Through use of Eqs. (9) and (12) the detector output current can be written as

$$\begin{aligned} i(t) &= \mathrm{Re}\, e^{-j(\omega_1-\omega_2)t}\int_A e^{j(k_1 r_1 - k_2 r_2)}\,dA \\ &= \mathrm{Re}\, e^{-j(\omega_1-\omega_2)t} e^{j(k_1 r_1' - k_2 r_2')}\int_A e^{jf(x,y)}\,dA, \end{aligned} \tag{14}$$

where

$$f(x, y) = (-k_1 \cos\theta_1 + k_2 \cos\theta_2)x + (-k_1 \cos\varphi_1 + k_2 \cos\varphi_2)y + \left(\frac{k_1}{2r_1'} \sin^2\theta_1 - \frac{k_2}{2r_2'} \sin^2\theta_2\right)x^2 + \left(\frac{k_1}{2r_1'} \sin^2\varphi_1 - \frac{k_2}{2r_2'} \sin^2\varphi_2\right)y^2 + \left(\frac{1}{r_1'} \cos\theta_1 \cdot \cos\varphi_1 - \frac{1}{r_2'} \cos\theta_2 \cdot \cos\varphi_2\right)xy + \cdots . \quad (15)$$

The problem of determining the output current when two coherent light beams strike upon a detector has been reduced to evaluating Eq. (14). When the quadratic and higher order terms in Eq. (15) are neglected, the light incident upon the detector from each source is effectively a plane wave. The detection problem is then equivalent to a Frunhofer diffraction problem.

3.1. The Rectangular Surface

When the detector of sides a and b is located in the Fraunhofer region of the light sources the output current is given by

$$\begin{aligned} i(t) &= \mathrm{Re}\, e^{-j(\omega_1-\omega_2)t} e^{j(k_1 r_1' - k_2 r_2')} \int_{-a/2}^{a/2} \int_{-b/2}^{b/2} e^{jf(x,y)} dx \cdot dy \\ &= \mathrm{Re}\, e^{-j[(\omega_1-\omega_2)t - (k_1 r_1' - k_2 r_2')]} \\ &\quad \times \int_{-a/2}^{a/2} e^{j[-k_1\cos\theta_1 + k_2\cos\theta_2]x} dx \int_{-b/2}^{b/2} e^{j[-k_1\cos\varphi_1 + k_2\cos\varphi_2]y} dy \\ &= ab\, D(\theta_1, \theta_2, \varphi_1, \varphi_2) \cos\left[(\omega_1-\omega_2)t - \phi\right], \end{aligned} \quad (16)$$

where

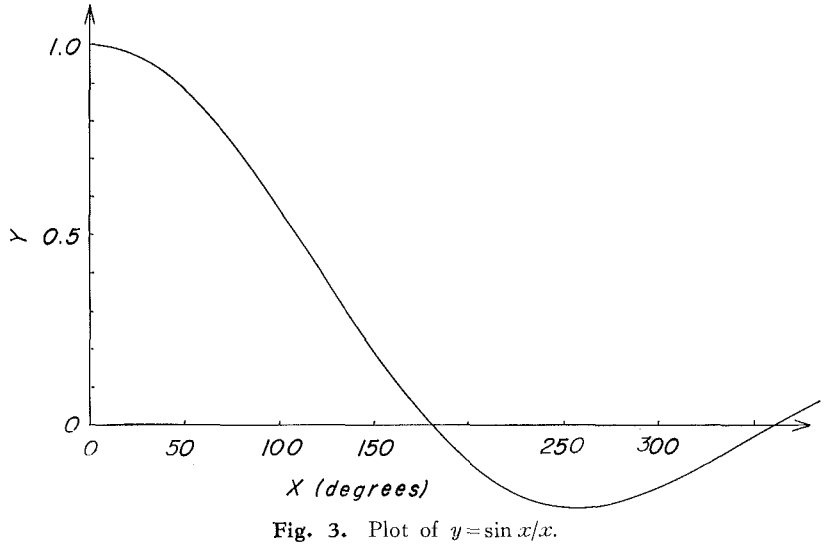

Fig. 3. Plot of $y = \sin x/x$.

$$\left.\begin{aligned} D(\theta_1, \theta_2, \varphi_1, \varphi_2) &= \frac{\sin(pa/2)}{pa/2} \cdot \frac{\sin(qb/2)}{qb/2}, \\ p &= -k_1 \cos\theta_1 + k_2 \cos\theta_2, \\ q &= -k_1 \cos\varphi_1 + k_2 \cos\varphi_2, \\ \phi &= k_1 r_1' - k_2 r_2'. \end{aligned}\right\} \tag{17}$$

$D(\theta_1, \theta_2, \varphi_1, \varphi_2)$ is the directivity factor and a plot of $\sin x/x$ is shown in Fig. 3.

Now consider two special cases of interest. The first special case is that in which $\theta_1 = \varphi_1 = \pi/2$. This corresponds to aligning one beam so that its equivalent point of origin is on the line perpendicular to the detector and passing through the detector center (Fig. 4). The local oscillator in an optical superheterodyne receiver might be so located. In this case p and q become

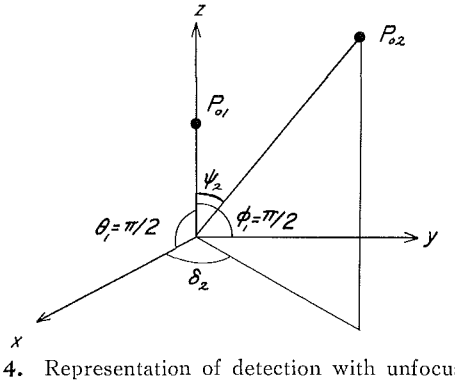

Fig. 4. Representation of detection with unfocused light in the case in which $\theta_1 = \varphi_1 = \pi/2$.

$$\left.\begin{aligned} p &= k_2 \sin\psi_2 \cdot \cos\delta_2, \\ q &= k_2 \sin\psi_2 \cdot \sin\delta_2. \end{aligned}\right\} \tag{18}$$

It is apparent that the required condition for negligible reduction in coherent detection can be calculated by

$$D(\theta_1, \theta_2, \varphi_1, \varphi_2) \geqq 1/\sqrt{2}. \tag{19}$$

Figure 5 shows the angular selectivity of δ_2 and ψ_2 for Eq. (19) in the case where $ab = 1\ \mathrm{cm}^2$ and $ab = 2\ \mathrm{cm}^2$ at $\lambda_2 = 1\ \mu$. For example if two light sources transmit at $1\ \mu$ and impinge at angles $\theta_1 = \varphi_1 = \pi/2$, $\delta_2 = 0$ and ψ_2 on a detector surface whose effective mixing area is the square of side 1 cm the two beams must be parallel to within about $\psi_2 = 2.54 \times 10^{-3}$ deg. In the rectangle of sides $a = 2$ cm and $b = 1$ cm, $\psi_2 = 1.27 \times 10^{-3}$ deg. This is a very stringent angle

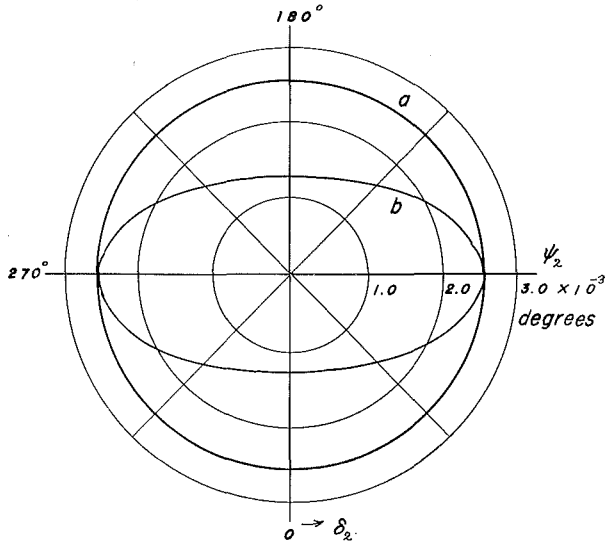

Fig. 5. The angular selectivity of δ_2 and ψ_2 for $D(\theta_1, \theta_2, \varphi_1, \varphi_2) \geqq 1/\sqrt{2}$ in the rectangular photosensitive surfaces at $\lambda_2 = 1\,\mu$ and $\theta_1 = \varphi_1 = \pi/2$; (a) $a = 1$ cm, $b = 1$ cm (b) $a = 1$ cm, $b = 2$ cm.

limitation. For large angle differences, the difference frequency output current will be more or less totally suppressed by the directivity factor $D(\theta_1, \theta_2, \varphi_1, \varphi_2)$.

The second special case of interest is that in which $\theta_1 = \theta_2 = \theta$ and $\varphi_1 = \varphi_2 = \varphi$. This condition means exactly parallel and non-normal incidence beams. Then p and q reduce

$$\left.\begin{aligned} p &= (k_2 - k_1) \sin\phi \cdot \cos\delta\,, \\ q &= (k_2 - k_1) \sin\phi \cdot \sin\delta\,. \end{aligned}\right\} \tag{20}$$

where $\phi_1 = \phi_2 = \phi$ and $\delta_1 = \delta_2 = \delta$. As a numerical example, let the wavelength $\lambda_1 = \lambda_2 + \Delta\lambda$, the rectangular surface of sides $a = 2$ cm and $b = 1$ cm, $\Delta f = 150$ MHz and $\delta = 0$. Then $\sin\phi = 44$, which, is of course impossible. The result means that as ϕ ranges from 0 to 90 deg. the operation is confined to a small region near the peak of the curve of $D(\theta_1, \theta_2, \varphi_3, \varphi_2)$. This result also points out that the detection of beats from exactly parallel beams is less critical to angular adjustment than the case in which one beam is aligned and the other is not. Namely if the two light beams are parallel, the angle at which they are incident upon the detector surface is not important.

3.2. The Circular Surface

In a similar way the output current can be investigated when the detector of a circular surface is located in the Fraunhofer region of the light sources. It is now approximated to use polar instead of rectangular coordinates. Let (ρ, δ) be the polar coordinates of a typical point:

$$x = \rho \cos \delta , \qquad y = \rho \sin \delta . \tag{21}$$

The function $f(x, y)$ now becomes

$$\begin{aligned} f(x, y) &= \rho \cos \delta(-k_1 \cos \theta_1 + k_2 \cos \theta_2) + \rho \sin \delta(-k_1 \cos \varphi_1 + k_2 \cos \varphi_2) \\ &= \rho\omega \cos (\delta - m) , \end{aligned} \tag{22}$$

where

$$\left.\begin{aligned} m &= \tan^{-1}(q/p) , \\ \omega^2 &= p^2 + q^2 . \end{aligned}\right\} \tag{23}$$

The output current now is given by, if ρ_0 is the radius of the circular surface,

$$i(t) = \mathrm{Re}\, e^{-j(\omega_1 - \omega_2)t} e^{j(k_1 r'_1 - k_2 r'_2)} \int_0^{\rho_0} \int_0^{2\pi} e^{j\omega\rho\cos(\delta - m)} \rho d\rho d\delta . \tag{24}$$

Now, we have the well-known integral representation of the Bessel Function $J_n(x)$:

$$J_n(x) = \frac{j^{-n}}{2\pi} \int_0^{2\pi} e^{jx\cos\alpha} e^{jn\alpha} d\alpha . \tag{25}$$

Equation (24) therefore reduces to

$$i(t) = 2\pi \cos\left[(\omega_1 - \omega_2)t - \phi\right] \int_0^{\rho_0} \rho J_0(\omega, \rho) d\rho . \tag{26}$$

Also, there is the well-known recurrence relation

$$\frac{d}{dx}\left[x^{n+1} J_{n+1}(x)\right] = x^{n+1} J_n(x) , \tag{27}$$

giving, for $n = 0$, on integration

$$\int_0^x x' J_0(x') dx' = x J_1(x) . \tag{28}$$

From Eqs. (26) and (28) it follows that

$$i(t) = \pi\rho_0^2 D(\omega, \rho_0) \cos\left[(\omega_1 - \omega_2)t - \phi\right] , \tag{29}$$

where

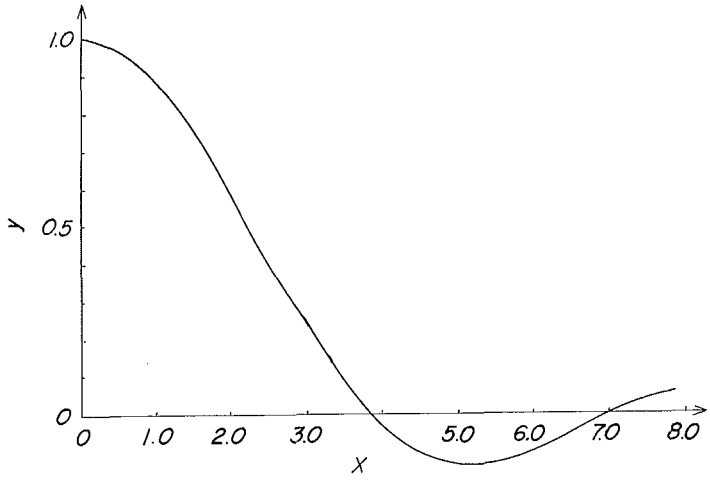

Fig. 6. Plot of $y=2J_1(x)/x$.

$$D(\omega, \rho_0) = \frac{2J_1(\omega, \rho_0)}{\omega\rho_0} . \tag{30}$$

The function $y=2J_1(x)/x$ is given in Fig. 6.

The first special case of interest is that in which $\theta_1=\varphi_1=\pi/2$. In this case ω reduces to

$$\omega = k_2 \sin\phi_2 . \tag{31}$$

It is apparent that the required condition for negligible reduction in output current can be calculated by

$$D(\omega, \rho_0) \geqq \frac{1}{\sqrt{2}} . \tag{32}$$

For example, if two beams transmit at $1\,\mu$ and impinge on a detection surface of radius $\rho_0=0.5$ cm, the two beams must be parallel to within about $\phi_2=2.96\times10^{-3}$ deg. This is a very severe angle limitation. For large angle difference, the output current will be more or less totally suppresed by the directivity factor $D(\omega, \rho_0)$. The second special case is that in which $\theta_1=\theta_2=\theta$ and $\varphi_1=\varphi_2=\varphi$. Then ω becomes

$$\omega = (k_2-k_1)\sin\phi . \tag{33}$$

As a numerical example, let the circular detector of radius $\rho_0=0.5$ cm and $\Delta f=150$ MHz. Then $\sin\phi=80$, which, is of course impossible. This means that if the two beams are parallel, the angle at which they are incident upon the detection surface is not important.

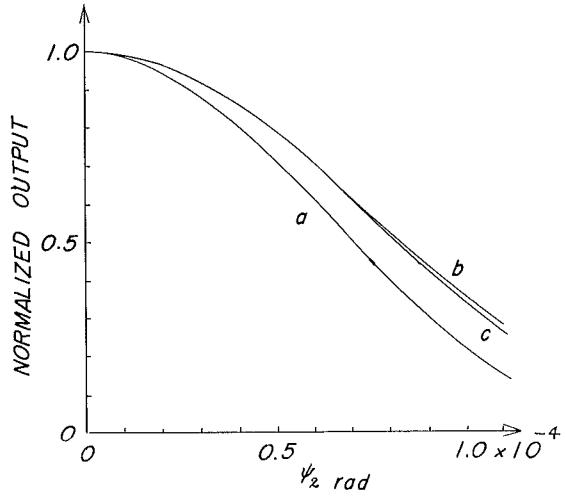

Fig. 7. The theoretical normalized output $[D(\psi_2)/D(0)]^2$ vs ψ_2 in the case where $\theta_1=\varphi_1=\pi/2$ and $\delta_2=0$ at 6328 Å; (a) the rectangular detector of sides $a=b=0.4$ cm, (b) the circular detector of radius $\rho_0=0.2$ cm, and (c) the rectangular detector of the same area with (b).

When $\theta_1=\varphi_1=\pi/2$, $\delta_2=0$, $a=b=0.4$ cm and $\rho_0=0.2$ cm at 6328 Å, plots of the normalized output as a function of ψ_2 are presented in Fig. 7 in the case of rectangular and circular detectors.

4. Focused Beams

4.1. Beams Focused by a Single Aperture

If the light is considered to pass through a single focusing system, which can be indicated schematically as a lens, then the problem can be represented as in Fig. 8. The lens is located in the $z=0$ plane and the detector in the $z=z$ plane, both centered at $x=y=0$. The field at the detector surface is now a supperposition of two fields which have been diffracted by the lens. The lens is assumed to be in the Fraunhofer region or far field of the light sources. That is, the light inci-

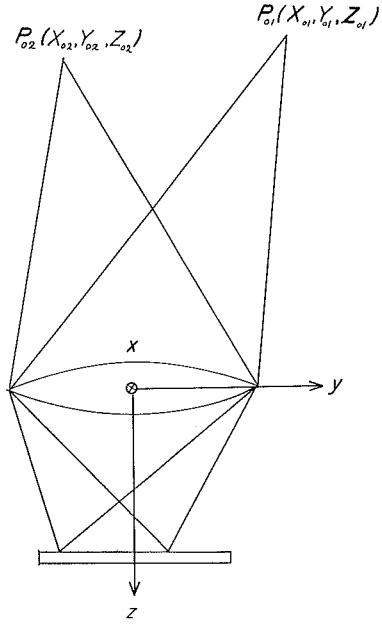

Fig. 8. Representation of detection process with focused light beams with a single aperture.

dent upon the aperture is effectively in the form of plane waves. Thus, the fields at the detector surface vary spatially as Fraunhofer diffraction patterns.

The field at the detector surface is

$$V(P_2, t) = E_1 e^{-j\omega_1 t} + E_2 e^{-j\omega_2 t}, \tag{34}$$

where

$$E_n = \int_{\text{aperture}} e^{jk_n(r_n+s)} dS. \tag{35}$$

The distance r_n from a point P_{0n} to a point Q on the aperture is

$$\begin{aligned} r_n &= \left[(\xi - X_{0n})^2 + (\eta - Y_{0n})^2 + Z_{0n}^2\right]^{1/2} \\ &= (r_n'^2 - 2\xi X_{0n} - 2\eta Y_{0n} + \xi^2 + \eta^2)^{1/2}, \end{aligned} \tag{36}$$

where r_n' is given by Eq. (11). Also, the distance s from P on the detector to Q is

$$\begin{aligned} s &= \left[(x-\xi)^2 + (y-\eta)^2 + z^2\right]^{1/2} \\ &= (s'^2 - 2x\xi - 2y\eta + \xi^2 + \eta^2)^{1/2}, \end{aligned} \tag{37}$$

where

$$s'^2 = x^2 + y^2 + z^2. \tag{38}$$

Again, using the binominal theorem and retaining only the linear terms, Eqs. (36) and (37) become

$$r_n = r_n' - \xi \cos\theta_n - \eta \cos\varphi_n, \tag{39}$$

and

$$s = s' - \xi \frac{x}{s'} - \eta \frac{y}{s'}. \tag{40}$$

where θ_n and φ_n are given by Eq. (13).

The spatial variation of the field at the surface of the detector becomes, by substituting Eqs. (39) and (40) into Eq. (35)

$$E_n(x, y) = \int_{\text{aperture}} e^{-jk_n(\xi\cos\theta_n + \eta\cos\varphi_n + \xi\frac{x}{s'} + \eta\frac{y}{s'})} d\xi \cdot d\eta. \tag{41}$$

Again the constants are dropped. Now Eq. (7) can be recongnized to be the form

$$i(t) = \mathrm{Re}\, e^{-j(\omega_1-\omega_2)t} F(0, 0), \tag{42}$$

where

$$F(\alpha, \beta)=\int_{-\infty}^{\infty} E_1(x, y)\cdot E_2^*(x, y)e^{j2\pi(\alpha x+\beta y)}dx\cdot dy\,, \tag{43}$$

is essentially the total of the radiation falling on the detector surface.

By rearranging the terms in Eq. (41), in the case of a rectangular aperture of sides ξ_a and η_a,

$$\begin{aligned} E_n(x, y) &= \int_{-\xi_a/2}^{\xi_a/2}\int_{-\eta_a/2}^{\eta_a/2} e^{-jk_n(\xi\cos\theta_n+\eta\cos\varphi_n+\frac{\xi x}{s'}+\frac{\eta y}{s'})}\,d\xi\cdot d\eta \\ &= \int_{-\xi_a/2}^{\xi_a/2}\left[G(\xi)e^{-jk_n\cos\theta_n\cdot\xi}\right]e^{-jk_n\xi\frac{x}{s'}}\,d\xi \\ &\quad\times\int_{-\eta_a/2}^{\eta_a/2}\left[G(\eta)e^{-jk_n\cos\varphi_n\cdot\eta}\right]e^{-jk_n\eta\frac{y}{s'}}\,d\eta\,, \end{aligned} \tag{44}$$

where

$$G(\xi)=G(\eta)=1\,. \tag{45}$$

By making a change of variables,

$$\begin{aligned} &\int_{-\xi/2}^{\xi_a/2}\left[G(\xi)e^{-jk_n\cos\theta_n\cdot\xi}\right]e^{-jk_n\xi\frac{x}{s'}}\,d\xi \\ &= \lambda_n s'\int_{-\xi_a/2\lambda_n s'}^{\xi_a/2\lambda_n s'} G(\chi\lambda_n s')e^{-jk_n\cos\theta_n\cdot\chi\lambda_n s'}e^{-j2\pi\chi x}\,d\chi \\ &= \int_{-\infty}^{\infty} G_n(\chi)e^{-j2\pi\chi x}\,d\chi\equiv E_n(x)\,, \end{aligned} \tag{46}$$

where

$$\left.\begin{aligned} G_n(\chi) &= \lambda_n s'\,e^{-jk_n\cos\theta_n\cdot\xi}\,, && \text{when} \quad |\xi|\leqq\xi_a/2\,, \\ &= 0\,, && \text{when} \quad |\xi|>\xi_a/2\,, \end{aligned}\right\} \tag{47}$$

and

$$\xi=\chi\lambda_n s'\,. \tag{48}$$

In the same way it follows that

$$\begin{aligned} &\int_{-\eta_a/2}^{\eta_a/2}\left[G(\eta)e^{-jk_n\cos\varphi_n\cdot\eta}\right]e^{-jk_n\eta\frac{y}{s'}}\,d\eta \\ &= \int_{-\infty}^{\infty} G_n(\tau)e^{-j2\pi\tau y}\,d\tau\equiv E(y)\,, \end{aligned} \tag{49}$$

where

$$\left.\begin{aligned} G_n(\tau) &= \lambda_n s'\,e^{-jk_n\cos\varphi_n\cdot\eta}\,, && \text{when} \quad |\eta|\leqq\eta_a/2\,, \\ &= 0\,, && \text{when} \quad |\eta|>\eta_a/2\,, \end{aligned}\right\} \tag{50}$$

and

$$\eta = \tau\lambda_n s' . \tag{51}$$

Then Eq. (44) can be rewritten as

$$\begin{aligned} E_n(x, y) &= \int_{-\infty}^{\infty} G_n(\chi) e^{-j2\pi\chi x} d\chi \int_{-\infty}^{\infty} G_n(\tau) e^{-j2\pi\tau y} d\tau , \\ &= E_n(x) E_n(y) . \end{aligned} \tag{52}$$

Equation (52) can be viewed to be in the form of a Fourier transform of the aperture function phase shifted by $k_n \cos\theta_n \chi\lambda_n s'$ and $k_n \cos\varphi_n \tau\lambda_n s'$ and changed from ξ_a and η_a to $\xi_a/\lambda_n s'$ and $\eta_a/\lambda_n s'$ in size. From a convolution in Fourier transform theory it can be shown that

$$\begin{aligned} F(\alpha, \beta) &= \int_{-\infty}^{\infty} E_1(x, y) \cdot E_2^*(x, y) e^{-j2\pi(\alpha x + \beta y)} dx \cdot dy \\ &= \int_{-\infty}^{\infty} E_1(x) \cdot E_2^*(x) e^{j2\pi\alpha x} dx \int_{-\infty}^{\infty} E_1(y) \cdot E_2^*(y) e^{j2\pi\alpha y} dy \\ &= \int_{-\infty}^{\infty} G_1(\alpha + \chi) \cdot G_2^*(\chi) d\chi \int_{-\infty}^{\infty} G_1(\beta + \tau) \cdot G_2^*(\tau) d\tau , \end{aligned} \tag{53}$$

where $G_n(\chi)$ and $E_n(x)$ are transform pairs and $G_n(\tau)$ and $E_n(y)$ are transform pairs.

From Eqs. (42) and (53), the expression for the current becomes

$$i(t) = \mathrm{Re}\, e^{-j(\omega_1 - \omega_2)t} \int_{-\infty}^{+\infty} G_1(\chi) \cdot G_2^*(\chi) d\chi \int_{-\infty}^{+\infty} G_1(\tau) \cdot G_2^*(\tau) d\tau , \tag{54}$$

When Eqs. (47) and (50) are substituted into Eq. (54),

$$\begin{aligned} i(t) = \mathrm{Re}\, e^{-j(\omega_1 - \omega_2)t} & \int_{-\xi_a/2\lambda_2 s'}^{\xi_a/2\lambda_2 s'} \exp\left[-j(k_1 \cos\theta_1 \cdot \lambda_1 s' - k_2 \cos\theta_2 \cdot \lambda_2 s')\right] \chi d\chi \\ & \times \int_{-\eta_a/2\lambda_2 s'}^{\eta_a/2\lambda_2 s'} \exp\left[-j(k_1 \cos\varphi_1 \cdot \lambda_1 \cdot s' - k_2 \cos\varphi_2 \cdot \lambda_2 s')\right] \tau d\tau , \end{aligned} \tag{55}$$

where λ_1 is assumed to be less than λ_2 and the unessential constant factor has been ignored. The current then becomes

$$i(t) = D_{sa} \cos(\omega_1 - \omega_2)t , \tag{56}$$

where

$$D_{sa} = \frac{\sin[(\cos\theta_1 - \cos\theta_2)\xi_a \pi/\lambda_2]}{(\cos\theta_1 - \cos\theta_2)\xi_a \pi/\lambda_2} \cdot \frac{\sin[(\cos\varphi_1 - \cos\varphi_2)\eta_a \pi/\lambda_2]}{(\cos\varphi_1 - \cos\varphi_2)\eta_a \pi/\lambda_2} , \tag{57}$$

which is similar in form to the unfocused Fraunhofer problem in the case of the rectangular detector surface.

When $\theta_1 = \varphi_1 = \pi/2$, then from Eq. (57)

$$D_{sa}=\frac{\sin[k_2\xi_a\cos\theta_2/2]}{k_2\xi_a\cos\theta_2/2}\cdot\frac{\sin[k_2\eta_a\cos\varphi_2/2]}{k_2\eta_a\cos\varphi_2/2}. \tag{58}$$

This result is identical to the result for $\theta_1=\varphi_1=\pi/2$ in the unfocused case except that ξ_a and η_a have replaced a and b, respectively. When $\theta_1=\theta_2=\theta$ and $\varphi_1=\varphi_2=\varphi$, it follows that

$$D_{sa}=1\,, \tag{59}$$

which indicates that the current is effectively independent of incidence angle within the range for which the assumption of analysis are valid.

Focusing, therefore, with a single effective aperture tends to increase the directivity when the aperture intercepts more light than the detector surface. If two beams are unfocused they completely overlap at the detector; however, when coming in at different angles they focus at different points, thus reducing the mixing effect. Inserting the lens is equivalent to changing the aperture, and as the aperture increases in the coherent detection process the directivity increases. When detecting coangular signals, then focusing the incident beam tends to remove any angular dependence by removing any phase variation across the detector surface regardless of frequency separation.

4.2. Beams Focused by Two Apertures

The result of Sec. 4.1 is concerned with the effect of focusing light beams with a single rectangular aperture of sides ξ_a and η_a, this shows that the directional pattern is narrowed as the aperture is increased because the size of the images has been decreased. Now, consider the case where two rectangular apertures are used and are translated so that the images remain fixed as the angle of incidence changes[11].

The schematic representation of the problem is shown in Fig. 9. The lenses are located in the $z=0$ plane centered at ξ_{01}, η_{01}, ξ_{02} and η_{02}, and the detector is in the $z=z$ plane centered at $x=y=0$. The coordinate axes ξ_1', η_1' and z are oriented at ξ_{01} and η_{01} in the $z=0$ plane and the coordinate axes ξ_2', η_2' and z are oriented at ξ_{02} and η_{02} in the $z=0$ plane. The distance from P_{01} to a point Q_1 on the first aperture is given by

$$\begin{aligned}r_1^2&=(X_{01}-\xi)^2+(Y_{01}-\eta)^2+Z_{01}^2\\&=\left[X_{01}-(\xi_{01}+\xi_1)\right]^2+\left[Y_{01}-(\eta_{01}+\eta_1)\right]^2+Z_{01}^2\\&=r_1'^2-2\xi_1(X_{01}-\xi_{01})^2-2\eta_1(Y_{01}-\eta_{01})^2+\xi_1^2+\eta_1^2\,,\end{aligned} \tag{60}$$

where

$$r_1'^2=(X_{01}-\xi_{01})^2+(Y_{01}-\eta_{01})^2+Z_{01}^2\,, \tag{61}$$

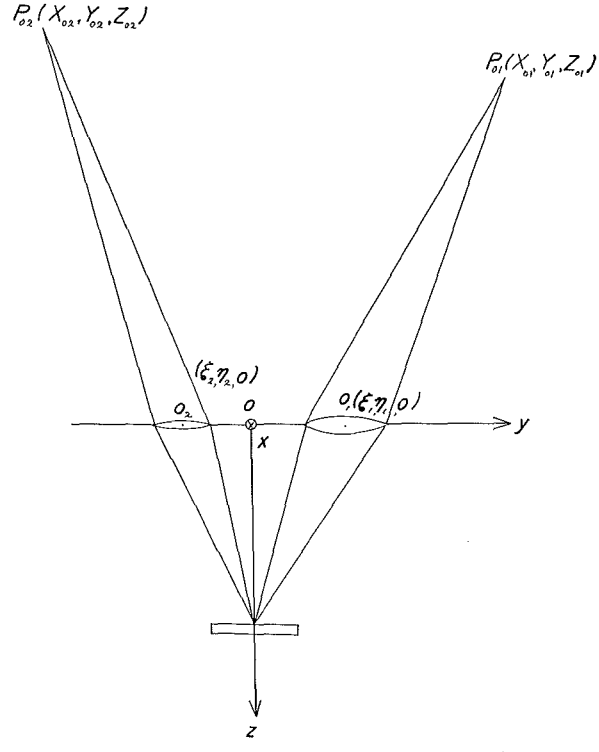

Fig. 9. Representation of detection process in which two apertures are used and are translated so that the images remain fixed as the angle of incidence changes.

and the distance from P of the detector to Q_1 is

$$\begin{aligned} s_1^2 &= (x-\xi)^2+(y-\eta)^2+z^2 \\ &= \left[x-(\xi_{01}+\xi_1)\right]^2+\left[y-(\eta_{01}+\eta_1)\right]^2+z^2 \\ &= s_1'^2-2x(\xi_{01}+\xi_1)-2y(\eta_{01}+\eta_1)+\xi_1^2+\eta_1^2 \\ &\quad +x^2+y^2+2\xi_{01}\xi_1+2\eta_{01}\eta_1 , \end{aligned} \tag{62}$$

where

$$s_1'^2 = \xi_{01}^2+\eta_{01}^2+z^2 . \tag{63}$$

With the aid of the binominal theorem it follows that

$$r_1 = r_1' - \frac{\xi_1(X_{01}-\xi_{01})}{r_1'} - \frac{\eta_1(Y_{01}-\eta_{01})}{r_1'} , \tag{64}$$

and

$$s_1 = s_1' - \frac{1}{s_1'}(\xi_{01}x + \xi_1 x + \eta_{01}y + \eta_1 y - \xi_{01}\xi_1 - \eta_{01}\eta_1)\,. \tag{65}$$

With the fact that

$$\left.\begin{aligned} \cos\theta_1 &= (X_{01} - \xi_{01})/r_1' = \xi_{01}/s_1'\,, \\ \cos\varphi_1 &= (Y_{01} - \eta_{01})/r_1' = \eta_{01}/s_1'\,, \end{aligned}\right\} \tag{66}$$

$r_1 + s_1$ can be written as

$$r_1 + s_1 = r_1' + s_1' - x\cos\theta_1 - y\cos\varphi_1 - \frac{\xi_1 x}{s_1'} - \frac{\eta_1 y}{s_1'}\,. \tag{67}$$

The spatial variation of the field at the detector surface is given by

$$E_n = \int_{\text{aperture}} e^{jk_n(r_n + s_n)}\,dS\,. \tag{68}$$

In the case of a rectangular of sides ξ_{an} and η_{an}, E_n can be written as

$$\begin{aligned} E_n &= \int_{-\xi_{an}/2}^{\xi_{an}/2}\int_{-\eta_{an}/2}^{\eta_{an}/2} e^{-jk_n(x\cos\theta_n + y\cos\varphi_n + \frac{\xi_n x}{s_n'} + \frac{\eta_n y}{s_n'})}\,d\xi_n d\eta_n \\ &= \left[e^{-jk_n x\cos\theta_n}\int_{-\infty}^{\infty} G_n(\chi_n)e^{-j2\pi\chi_n x}\,d\chi_n\right] \\ &\quad \times \left[e^{-jk_n y\cos\theta_n}\int_{-\infty}^{\infty} G_n(\tau_n)e^{-j2\pi\tau_n y}\,d\tau_n\right] \\ &= G_n(x)e^{-jk_n x\cos\theta_n}\cdot G_n(y)e^{-jk_n y\cos\varphi_n}\,, \end{aligned} \tag{69}$$

where

$$\left.\begin{aligned} G_n(\xi_n) &= 1 \quad \text{when} \quad |\xi_n| \leqq \xi_{an}/2\,, \\ &= 0 \quad \text{when} \quad |\xi_n| > \xi_{an}/2\,, \end{aligned}\right\} \tag{70}$$

$$\left.\begin{aligned} G_n(\eta_n) &= 1 \quad \text{when} \quad |\xi_n| \leqq \xi_{an}/2\,, \\ &= 0 \quad \text{when} \quad |\eta_n| > \xi_{an}/2\,, \end{aligned}\right\} \tag{71}$$

and

$$\xi_n = \chi_n\lambda_n s_n'\,, \qquad \eta_n = \tau_n\lambda_n s_n'\,. \tag{72}$$

Now the output current is given by

$$\begin{aligned} i(t) &= \text{Re}\, e^{-j(\omega_1 - \omega_2)t}\int_{-\infty}^{\infty} E_1\cdot E_2^*\,dx\,dy \\ &= \text{Re}\, e^{-j(\omega_1 - \omega_2)t}\int_{-\infty}^{\infty}\exp\left[j2\pi\left(\frac{\cos\theta_2}{\lambda_2} - \frac{\cos\theta_1}{\lambda_1}\right)x\right]G_1(x)\cdot G_2^*(x)dx \\ &\quad \times \int_{-\infty}^{\infty}\exp\left[j2\pi\left(\frac{\cos\varphi_2}{\lambda_2} - \frac{\cos\varphi_1}{\lambda_1}\right)y\right]G_1(y)\cdot G_2^*(y)dy \end{aligned} \tag{73}$$

from Eq. (59).

And by use of a convolution in Fourier transform it can be shown that

$$i(t) = \mathrm{Re}\, e^{-j(\omega_1-\omega_2)t}\int_{-\infty}^{\infty} G_1\left[\left(\frac{\cos\theta_2}{\lambda_2}-\frac{\cos\theta_1}{\lambda_1}\right)+\chi\right]\cdot G_2^*(\chi)d\chi$$
$$\times\int_{-\infty}^{\infty} G_1\left[\left(\frac{\cos\varphi_2}{\lambda_2}-\frac{\cos\varphi_1}{\lambda_1}\right)+\tau\right]\cdot G_2^*(\tau)d\tau \tag{74}$$

since $G_n(x)$ and $G_n(\chi)$ are transform pairs and $G_n(y)$ and $G_n(\tau)$ are transform pairs. Equation (74) indicates that the angular sensitivity may be obtained by evaluating a convolution integral at particular values of θ_1, φ_1, θ_2 and φ_2. From Eqs. (70) and (71),

$$\left.\begin{aligned} G_1(\chi) &= 1 \quad \text{when} \quad |\chi| \leqq \xi_{a1}/2\lambda_1 s_1', \\ G_2(\chi) &= 1 \quad \text{when} \quad |\chi| \leqq \xi_{a2}/2\lambda_2 s_2', \end{aligned}\right\} \tag{75}$$

and

$$\left.\begin{aligned} G_1(\tau) &= 1 \quad \text{when} \quad |\tau| \leqq \eta_{a1}/2\lambda_2 s_2', \\ G_2(\tau) &= 1 \quad \text{when} \quad |\tau| \leqq \eta_{a2}/2\lambda_2 s_2'. \end{aligned}\right\} \tag{76}$$

A plot of

$$D(\rho) = \int_{-\infty}^{\infty} G_1(\rho+\chi)\cdot G_2^*(\chi)d\chi \tag{77}$$

is shown in Fig. 10. The expression goes to zero at

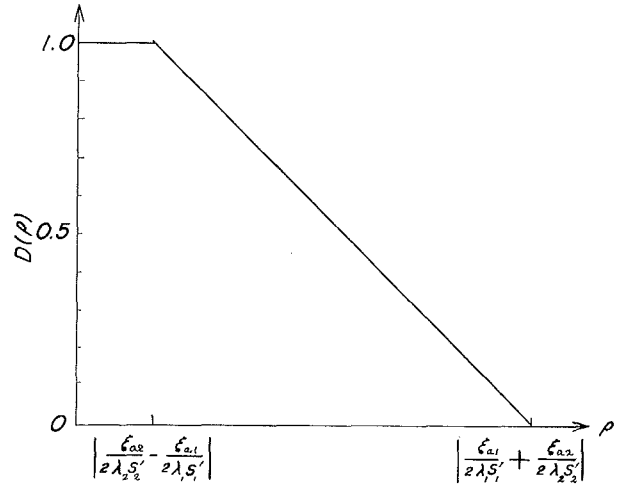

Fig. 10. Plot of convolution integral for Eq. (77).

$$\rho = \frac{\cos\theta_2}{\lambda_2} - \frac{\cos\theta_1}{\lambda_1} = \left| \frac{\xi_{a1}}{2\lambda_1 s_1'} - \frac{\xi_{a2}}{2\lambda_2 s_2'} \right|, \tag{78}$$

When $\theta_1 = \varphi_1 = \pi/2$ and $\xi_{a1}\lambda_2 s_2' = \xi_{a2}\lambda_1 s_1'$ and $\delta_2 = 0$ the tolerance on the angular difference is

$$\sin\phi_2 = 0.586 \frac{\xi_{a1}}{2s_1'} . \tag{79}$$

As a numerical example, let $\xi_{a1} = 1$ cm and $s_1' = 100$ cm

$$\phi_2 = 1.67 \times 10^{-1} \text{ deg.} \tag{80}$$

This result indicates that the method of multiple focusing can make coherent detection relatively in sensitive to angular displacement and that, if the images of the focused beams are always overlapped, then the directional property is less sensitive to the angle. However, the condition that two beams overlap implies a critical alignment in actual devices. Read and Fried[13] have avoided this problem by making one beam much larger than the other. While the angular sensitivity becomes less critical, the efficiency of the detection process is reduced because some of the energy is not used and it also generates shot noise which is undesirable.

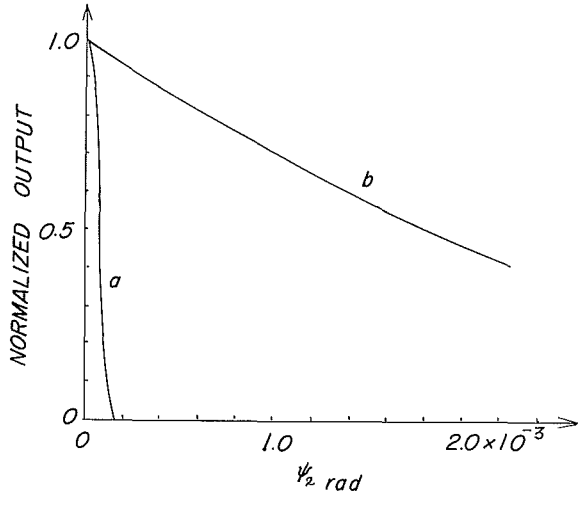

Fig. 11. The theoretical normalized output $[D(\psi_2)/D(0)]^2$ vs ψ_2 in the case where $\theta_1 = \varphi_1 = \pi/2$ and $\delta_2 = 0$ at 6328 Å; (a) unfocused light on the rectangular detector of sides $a = b = 0.4$ cm, and focused light with a single aperture of sides $\xi_0 = \eta_0 = 0.4$ cm and $s' = 65$ cm, (b) focused light with two apertures of $\xi_{a1} = \eta_{a1} = \xi_{a2} = \eta_{a2} = 0.4$ cm and $\lambda_1 = \lambda_2$.

When $\theta_1=\varphi_1=\pi/2$ and $\delta_2=0$ at 6328 Å calculated curves of the normalized output as a function ϕ_2 are shown in Fig. 11 in the case of unfocused light, focused beams with a single aperture, and focused beams with multiple apertures. It was assumed that $a=b=0.4$ cm for unfocused light, $\xi_a=\eta_a=0.4$ cm and $s'=65$ cm for focused light with a single aperture, and $\xi_{a1}=\eta_{a1}=\xi_{a2}=\eta_{a2}=0.4$ cm and $\lambda_1=\lambda_2$ for focused light with multiple apertures.

5. A Comparison of Theoretical and Experimental Values

To test the above theoretical predictions an experimental technique utilizing a beam splitter to separate the output of a single laser into a local oscillator and signal beam was used. Figure 12 shows that this homodyne system is

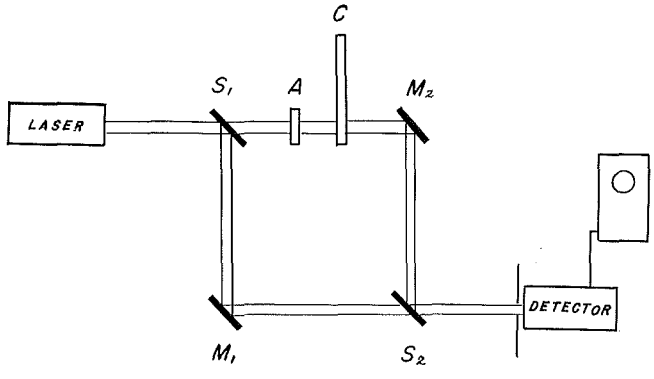

Fig. 12. Experimental setup.

basically a Mach-Zehnder interferometer. A collimated beam from a He–Ne laser was split in two portions, a "local oscillator" beam going towards mirror M_1, and a "signal" beam going towards mirror M_2. The signal beam is amplitude-modulated by a mechanical chopper C and attenuated by an optical attenuator A just before chopper C. The local oscillator and signal beams reflected by mirrors M_1 and M_2 were combined at the beam splitter S_2 and were detected. The laser used in this work was a 6328 Å He–Ne laser. Several different detectors were used, including a MS9S photomultiplier, a 7696 photomultiplier and LSD 39 photodiodes. The beam was passed through an aperture, finally impinging on the photosensitive surface and the output was amplified.

The output for unfocused light, normalized to a maximum value of 1, is shown in Fig. 13 in the case where the radius of aperture just before the photosensitive surface of MS9S photomultiplier is 1.5 mm and $\theta_1=\varphi_1=\pi/2$.

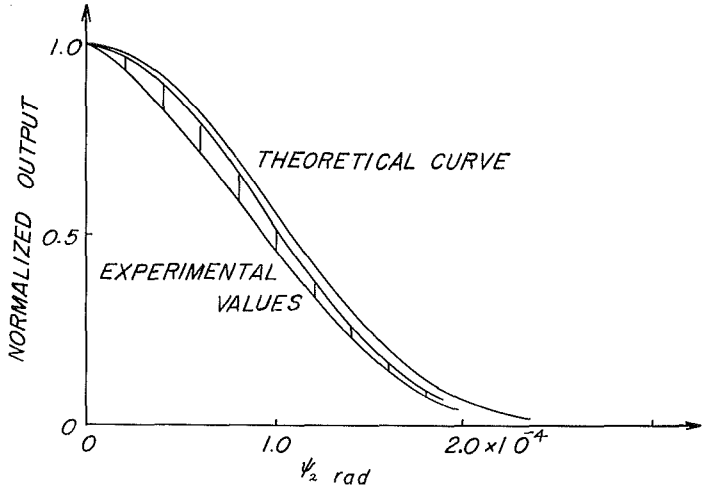

Fig. 13. Detected signal for unfocused light vs angular mismatch in the case in which the radius of the circular photosensitive surface is 1.5 mm and $\theta_1=\varphi_1=\pi/2$ and a MS9S photomultiplier is used.

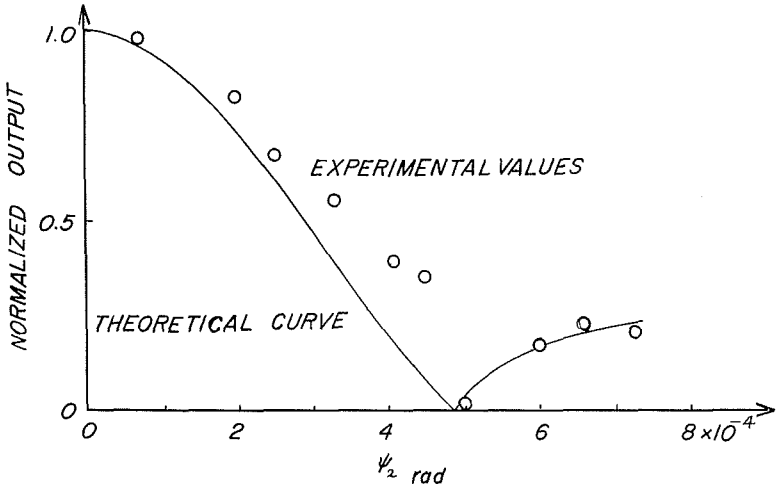

Fig. 14. Detected signal for unfocused light vs angular mismatch in the case where the rectangular photosensitive surface of sides $a=1.3$ mm and $b=2$ mm, $\theta_1=\varphi_1=\pi/2$, $\delta_2=0$ and a 7696 photomultiplier is used. (From Mr. K. Koyanagi).

The experimental values are in the shaded region and they accompany the theoretically expected curve as a function of angular misalignment. Figure 14 shows the normalized output as a function of angular misalignment in the case where the rectangular detector surafce of sides $a=1.3$ mm and $b=2.0$ mm and $\theta_1=\varphi_1=\pi/2$ and $\delta_2=0$. As seen from Figs. 13 and 14, good experimental confirmation for unfocused light is obtained with the optical homodyne system of rectangular and circular photosensitive surfaces.

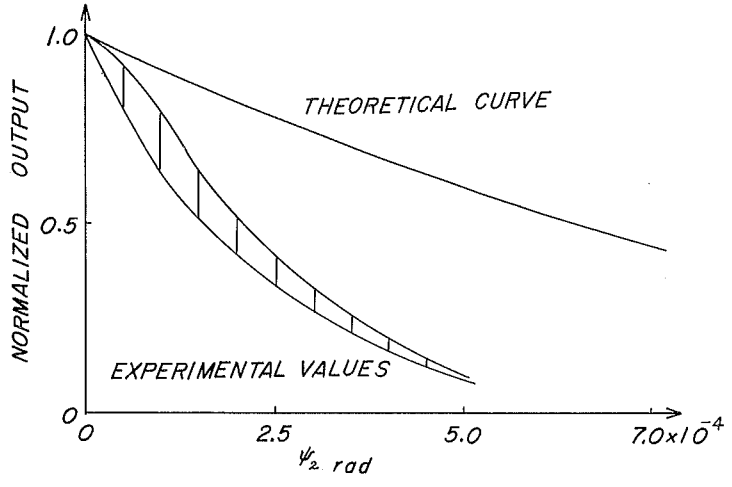

Fig. 15. Detected signal for focused light beams vs angular mismatch in the case in which the focal length of the focusing lens is 65 cm and the radius of the photosensitive surface is 1.5 mm and a MS9S photomultiplier is used. The discrepancy between theoretical and experimental values is caused by the short focal length.

When the focusing lense was placed just before the splitter S_1 experimental and theoretical values as a function of angular misalignment are shown in Fig. 15. The focal length of the focusing lens was 65 cm and the diameter of laser beam was 3 mm. The circular surface of radius 1.5 mm was located at 135 cm from the focusing lens. As seen from this figure, the theoretically expected curve of angular misalignment is somewhat larger than that of the experimental values. It is considered that this discrepancy was caused by the short focal length of the focusing lens. However, it should be noted from Figs. 13, 14 and 15 that as the angle of incidence changes the directional pattern is less sensitive to the angle.

6. Conclusions

In optical heterodyne detection processes, Corcoran's analysis in the directional characteristics of one-dimensional photosensitive surface was modified to two-dimensional detectors.

The directivity factors could be summarized as follows;

1) The directivity factor of a rectangular detector of sides a and b, $D(\theta_1, \theta_2, \varphi_1, \varphi_2)$, is given by $4\sin(pa/2)\cdot\sin(qb/2)/pqab$
2) The directivity factor of a circular detector of radius ρ_0 is shown by $D(\omega, \rho_0)=2J_1(\omega, \rho_0)/\omega\rho_0$.
3) The directivity factor of focusing light beams with a single rectangular aperture of sides ξ_a and η_a is in a similar form to the unfocused Fraunhofer problem, and the directional pattern is narrowed as the rectangular aperture is increased.
4) The directional pattern is less sensitive to angle when two rectangular apertures are used and translated so that the images remain fixed as the angle of incidence changes.
5) Good experimental confirmation was obtained with optical homodyne receivers.

Acknowledgement

The authors are indebted to Prof. A. Matsumoto, Prof. T. Kurobe, Prof. Y. Ozawa, Prof. M. Suzuki, Asst. Prof. A. Nishitsuji and Asst. Prof. Y. Aoki, for their valuable discussions on the Frunhofer problem at a meeting on March 5, 1968. Also, the authors are grateful to the staff of Chairs of Solid State Electronics, Applications of Electromagnetic Waves, Electronic Apparatus, Applied Optics, and Engineering Physics, for their helpful suggestions and for the use of their various apparatus. Lastly, the authors wish to thank Dr. Y. Kinoshita for his valuable suggestions in adjusting the experimental device, Asst. Prof. Y. Tochinai for his help in programming the digital computer, Mr. M. Senda and Mr. C. Fukuda for their helpful suggestions and Mr. K. Koyanagi for his experimental assistance in the CW laser experiment and for the use of Fig. 14.

References

1) Hutter, G. E.: "The microwave phototube, new detector for optical receivers," Electronics, vol. 35, pp. 37–41, July 20, 1962.
2) Jacobs, S.: "The optical heterodyne," Electronics, vol. 36, pp. 29–31, July 12, 1963.
3) Siegman, A. E., Harris, S. E. and McMurtry, B. J.: "Optical heterodying and optical demodulation at microwave frequencies," Proc. Symp. on Optical Maser,

Polytechnic Institute of Brooklyn, New York, pp. 511-527, April 1963.

4) Sakuraba, I.: "Analysis of O-type photoelectron beam demodulators for amplitude-modulated light signals," Bulletin of the Faculty of Engineering, Hokkaido University, Sapporo, Japan, No. 32, pp. 175-186, October 1963 (in Japanese).

5) Sakuraba, I. and Rowe, J. E.: "Photodemodulation of coherent light signals in centrifugal electrostatic focusing systems," Technical Report No. 75, Electron Physics Laboratory, Department of Electrical Engineering, The University of Michigan, Ann Arbor, Michigan, September 1964.

6) Sakuraba, I.: "Photomixing and photoelectron-beam demodulation for microwave amplitude-modulated light signals," Bulletin of the Faculty of Engineering, Hokkaido University, Sapporo, Japan, No. 41, pp. 95-120, August 1966 (in Japanese).

7) Oliver, B. M.: "Signal-to-noise ratios in photoelectric mixing," Proc. IRE, vol. 49, pp. 1960-1961, December 1961.

8) Haus, H, A., Townes, C. H. and Oliver, B. M.: "Comments on noise in photoelectric mixing," Proc. IRE, vol. 50, pp. 1544-1545, June 1962.

9) Jacobs, S. and Rabinowitz: "Optical heterodyning with a CW gaseous laser," Quantum Electronics, Columbia University Press, New York, pp. 481-487, 1964.

10) Rabinowitz, P., LaTourrette, J. and Gould, G.: "AFC optical heterodyne detector," Proc. IEEE, vol. 51, pp. 857-858, May, 1963.

11) Corcoran, V. J.: "Directional characteristics in optical heterodyne detection processes," J. Appl. Phys., vol. 36, pp. 1819-1825, June 1965.

12) Sakuraba, I. and Chida, H.: "Directivity of linear-photoelectron-beam systems in optical heterodyne detection processes," Bulletin of the Faculty of Engineering, Hokkaido University, Sapporo, Japan, No. 44, pp. 59-66, September 1967 (in Japanese).

13) Read, W. S. and Fried, D. L.: "Optical heterodying with noncritical angular alignment," Proc. IEEE vol. 51, p. 1787, December 1963.

14) Read, W. S. and Turner, R. G.: "Tracking heterodyne detection," Appl. Opt., vol. 4, p. 1570, December 1965.

15) Siegman, A. E.: "The antenna properties of optical heterodyne receiver," Proc. IEEE,. vol. 54, pp. 1350-1356, October 1966.

16) Lucy, R. F., Lang, K, Peters, C. J. and Duval, K.: "Optical superheterodyne receiver," Applied Optics, vol. 6, pp. 1333-1342, August 1967.

17) Brown, R. H. and Twiss, R. Q.: "Correlation between photons in two coherent beams of light," Nature, vol. 177, pp. 27-29, January 7, 1956.

18) Corcoran, V. J. and Pao, Y. H.: "Detection of laser radiation," J. Opt. Soc. Am., vol. 52, pp. 1341-1350, December 1962.

19) Forrester, A. T.: "Photodetection and photomixing of laser output," Advances in Quantum Electronics, Columbia University Press, New York, pp. 233-238, 1961.

20) Born, M. and Wolf, E.: "Principles of Optics," Third Edition, Pergamon Press, London, 1965.